CORONAVIRUS

Squalene-based multidrug nanoparticles for improved mitigation of uncontrolled inflammation in rodents

Flavio Dormont[1], Romain Brusini[1], Catherine Cailleau[1], Franceline Reynaud[1,2], Arnaud Peramo[1], Amandine Gendron[1], Julie Mougin[1], Françoise Gaudin[3,4], Mariana Varna[1], Patrick Couvreur[1]*

Uncontrolled inflammatory processes are at the root of numerous pathologies. Most recently, studies on confirmed COVID-19 cases have suggested that mortality might be due to virally induced hyperinflammation. Uncontrolled pro-inflammatory states are often driven by continuous positive feedback loops between pro-inflammatory signaling and oxidative stress, which cannot be resolved in a targeted manner. Here, we report on the development of multidrug nanoparticles for the mitigation of uncontrolled inflammation. The nanoparticles are made by conjugating squalene, a natural lipid, to adenosine, an endogenous immunomodulator, and then encapsulating α-tocopherol, as antioxidant. This resulted in high drug loading, biocompatible, multidrug nanoparticles. By exploiting the endothelial dysfunction at sites of acute inflammation, these multidrug nanoparticles delivered the therapeutic agents in a targeted manner, conferring survival advantage to treated animals in models of endotoxemia. Selectively delivering adenosine and antioxidants together could serve as a novel therapeutic approach for safe treatment of acute paradoxal inflammation.

INTRODUCTION

Uncontrolled inflammation is a key health challenge and is associated with numerous diseases (*1*–*3*). Recently, coronavirus disease 2019 (COVID-19) infections have been recognized as leading to a hyperinflammatory state characterized by a fulminant cytokine storm (hypercytokinemia) before acute respiratory distress syndrome and death (*4*). A growing understanding of the pathophysiology accompanying acute inflammation can help devise novel therapeutics for inflammatory diseases (*5*). Of particular relevance is that severe inflammation is associated with significant alterations to redox balance (*6*), inducing oxidative stress to tissues and cells. Evidence accumulated over the past two decades has pointed to significant connections between inflammation and oxidative stress, both processes contributing to fuel one another, thereby establishing a vicious cycle able to perpetuate and propagate the inflammatory response (*7*, *8*).

Inhibiting pathological inflammatory responses and the cross-talk between oxidative stress and inflammation presents various challenges (*9*). For instance, while potent anti-inflammatory agents—such as corticosteroids—already exist, these have fallen short in acute inflammatory conditions such as sepsis, because of their negative effects on tissue repair and the reported adrenocortical insufficiency common in patients with sepsis (*10*). Adenosine (Ad), an endogenous purine, and Ad receptor agonists have shown promise by promoting the resolution of inflammation (*11*, *12*), but their systemic administration is associated with rapid clearance (*13*) and unacceptable medical side effects related to untargeted activation of their cognate receptors (*14*, *15*). Another challenge consists in the fact that, during the evolution of systemic inflammatory insults, the initial response performed by the innate immune system is transferred from the plasma to tissues and cells where it results in disturbed signaling, cell dysfunction, and eventually organ failure. Therefore, efficient therapies against such processes need to be targeted to the inflammation sites. Similarly, antioxidant supplementation has been attempted (*16*–*18*) to scavenge reactive species during acute inflammation but remains limited by poor pharmacodynamics and tissue penetration (*19*). Recently, multidrug treatments of low-dose hydrocortisone with antioxidants have emerged as a promising approach for the mitigation of uncontrolled inflammation (*20*), simultaneously inhibiting pro-inflammatory cascades and scavenging reactive oxygen species (ROS). However, so far, most of the antioxidants used in this context perform their action predominantly in the plasma. While this is useful during the initial hyperinflammatory stages of the body response, it is ineffective at inhibiting the pathological redox cycles happening inside cells and tissues (*19*)—as plasma antioxidant levels poorly correlate with intracellular antioxidant levels (*21*).

To improve on these issues, and taking into account the potential of Ad and multidrug therapies for the resolution of inflammation, we propose here a novel prodrug-based nanoparticle (NP) formulation, enabling the targeted delivery of Ad and tocopherol (VitE) to the sites of acute inflammation. Recently, conjugation of therapeutic molecules to squalene (SQ), an endogenous lipid, has been shown to enhance blood circulation time (*22*), provide interesting targeting properties (*23*) and lower toxicity (*24*). Here, we show that the bioconjugation of Ad to SQ and further nanoformulation with VitE led to the formation of stable multidrug NPs allowing (i) efficient encapsulation of both drugs, (ii) reduced side effects, and (iii) promising anti-inflammatory and protective effects in models of endotoxemia and lethal systemic shock. Furthermore, we also report evidence that these SQ-based NPs could target inflamed tissues in multiple murine models of inflammation for selective Ad receptor activation and antioxidant action. These functionalities together enabled a therapeutic intervention with significant potential for the antioxidant management of acute inflammatory diseases and improved the use of Ad as a proresolving pharmaceutical agent.

[1]Institut Galien Paris-Sud, CNRS UMR 8612, Université Paris-Sud, Université Paris-Saclay, 92296 Châtenay-Malabry, France. [2]School of Pharmacy, Federal University of Rio de Janeiro, 21944-59 Rio de Janeiro, Brazil. [3]Plateforme d'Histologie Immunopathologie de Clamart (PHIC) Université Paris-Saclay, Inserm, CNRS, Institut Paris Saclay d'Innovation thérapeutique, 92296 Châtenay-Malabry, France. [4]Université Paris-Saclay, Inserm, Inflammation, Microbiome and Immunosurveillance, 92140 Clamart, France.
*Corresponding author. Email: patrick.couvreur@universite-paris-saclay.fr

RESULTS AND DISCUSSION

Preparation and characterization SQAd/VitE NPs

The preparation of squalene-Ad (SQAd)/VitE NPs first required conjugation of Ad to squalenic acid as previously described (*25*). This conjugation step was performed with moderate yield (45%) and afforded SQAd, which could then be used as a prodrug-based nanocarrier for VitE (Fig. 1A). The second step in the preparation of multidrug SQ-based NPs consisted in encapsulating VitE in SQAd NPs, which was performed by a nanoprecipitation technique. Following nanoprecipitation and solvent removal, the VitE content of the NPs was evaluated. For SQAd/VitE nanoformulations containing 50 weight % (wt %) VitE or less, most of the VitE present in the precursor organic solution was found to be incorporated in the NPs (Fig. 1B). For the rest of this study, we used the SQAd/VitE NP formulation, which afforded the highest total drug loading with proper colloidal stability, i.e., SQAd/VitE (50:50) wt %. The total drug loading of the multidrug NPs was therefore 68.6 wt %: 50 wt % VitE and 18.6 wt % Ad. When measured by dynamic light scattering (DLS), the multidrug SQAd/VitE NPs displayed a uniform size distribution with a mean hydrodynamic diameter of 71.2 ± 3 nm and a polydispersity index inferior to 0.2 (Fig. 1C). Surface zeta potential was measured to be −14.29 ± 1.01 (SEM) mV, similar to SQAd NP only (−15.45 ± 1.52 mV), ensuring proper colloidal stability (Fig. 1D). The obtained multidrug NPs were also observed by cryogenic transmission electron microscopy (cryo-TEM) imaging, revealing uniform NPs (Fig. 1E). Following their formulation, SQAd/VitE NPs were suspended in 50% serum and showed satisfactory colloidal stability over 5 days (Fig. 1F). To evaluate drug release, we measured the amount of free Ad and VitE released from the formulation over time by high-performance liquid chromatography (HPLC). The incubation of SQAd/VitE NPs in serum resulted in a slow, progressive decrease in detected SQAd bioconjugate, which correlated with a release of free Ad (Fig 1G). After 48 hours of incubation, about 6% of the initial Ad was found to have been released from SQAd/VitE NPs, while no VitE release could be detected (see Supplementary Discussion).

SQ is an endogenous precursor of cholesterol, which forms stable colloidal phases in water (*26*). VitE is insoluble in water and usually

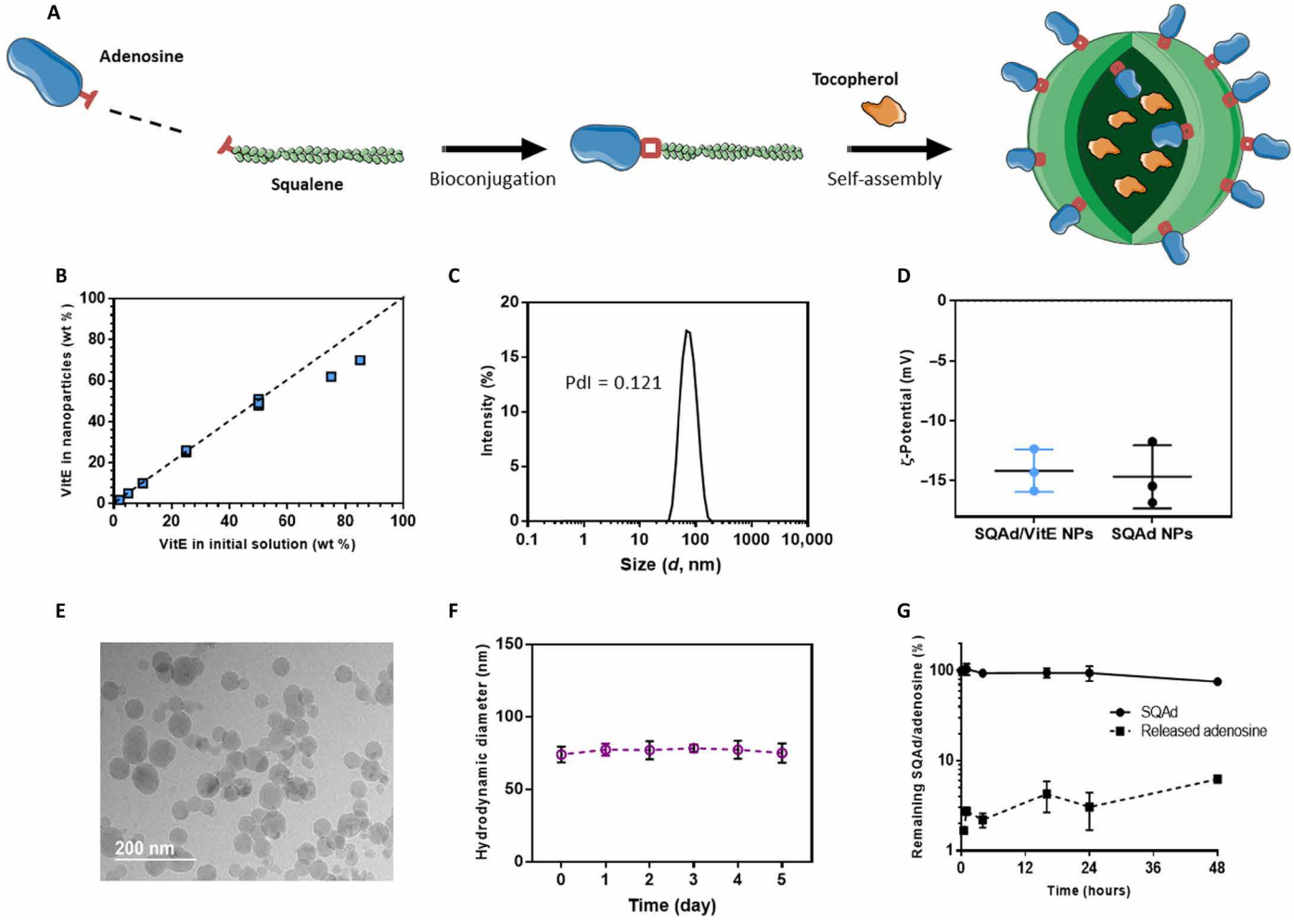

Fig. 1. Formulation and characterization of multidrug SQAd/VitE NPs. (**A**) Schematic representation of SQAd bioconjugation and VitE encapsulation to afford SQAd/VitE NPs. (**B**) VitE encapsulation efficiency in SQAd/VitE NPs as measured by high-performance liquid chromatography (HPLC). wt %, weight %. (**C**) Hydrodynamic size of SQAd/VitE NPs (diameter, nanometers) measured by DLS. Pdi, polydispersity index. (**D**) Measurement of surface ζ-potential of SQAd/VitE and SQAd NPs. (**E**) cryo-TEM images of SQAd/VitE NPs (scale bar, 200 nm). (**F**) Stability of SQAd/VitE NPs in 50% fetal bovine serum (FBS) over 5 days as measured by DLS. (**G**) Release of Ad from SQAd/VitE NPs in 50% FBS.

colocalizes with cholesterol in low-density lipoproteins (LDLs) in vivo (*27*). Accordingly, our results showed that VitE was efficiently encapsulated in SQAd NPs to form stable multidrug NPs. Overall, the preparation of SQAd/VitE NPs is very straightforward because it simply requires an ethanolic solution of SQAd and VitE to be added in water medium before ethanol evaporation. The total synthesis also did not require any excipients, which makes the scaling-up affordable as shown previously with the ability of SQAd bioconjugates to be produced as an industrial sample (*24*). Noteworthy, this may represent an asset over the current trend of developing ever more sophisticated nanomedicines, whose physicochemical complexity represents an important factor to slow the speed and even the feasibility of nanomedicine translation into the clinic.

NP tracking studies

To investigate whether SQ NPs could improve the bioavailability of the encapsulated therapeutic agents and direct them to the inflammation foci, we evaluated the in vivo biodistribution of SQAd/VitE NPs in two different models, one of local acute inflammation and one of systemic inflammation. First, the in vivo circulation of SQAd/VitE NPs was followed after intravenous injection of fluorescent DiD (1,1′-dioctadecyl-3,3,3′,3′-tetramethylindodicarbocyanine, 4-chlorobenzenesulfonate salt)–labeled SQAd/VitE NPs in a murine lipopolysaccharide (LPS)–induced paw inflammation model. Animals received 100 ng of LPS in their right paw and a control saline injection in the left paw. The fluorescence in tissues was monitored noninvasively up to 24 hours, from the abdomen side using an In Vivo Imaging System (IVIS) Lumina. The real-time in vivo imaging showed that, in comparison with the control healthy left paw, a strong increase in the radiant efficiency of the inflamed right paw could be detected after intravenous injection of fluorescent SQAd/VitE NPs (Fig. 2, A to E). In a control experiment, when the mice received a free DiD solution, no significant accumulation of fluorescence was observed in the inflamed paw (Fig. 2B) (see Supplementary Discussion). The relative fluorescence signals detected in the right (inflamed) paw versus left (noninflamed) paw of the studied animals can be found in fig. S4. In another control experiment, comparing the observed accumulation of SQ NPs with that of PLGA [poly(lactic-*co*-glycolic) acid] NPs, it was observed that the accumulation of SQAd/VitE NPs occurred faster, providing higher

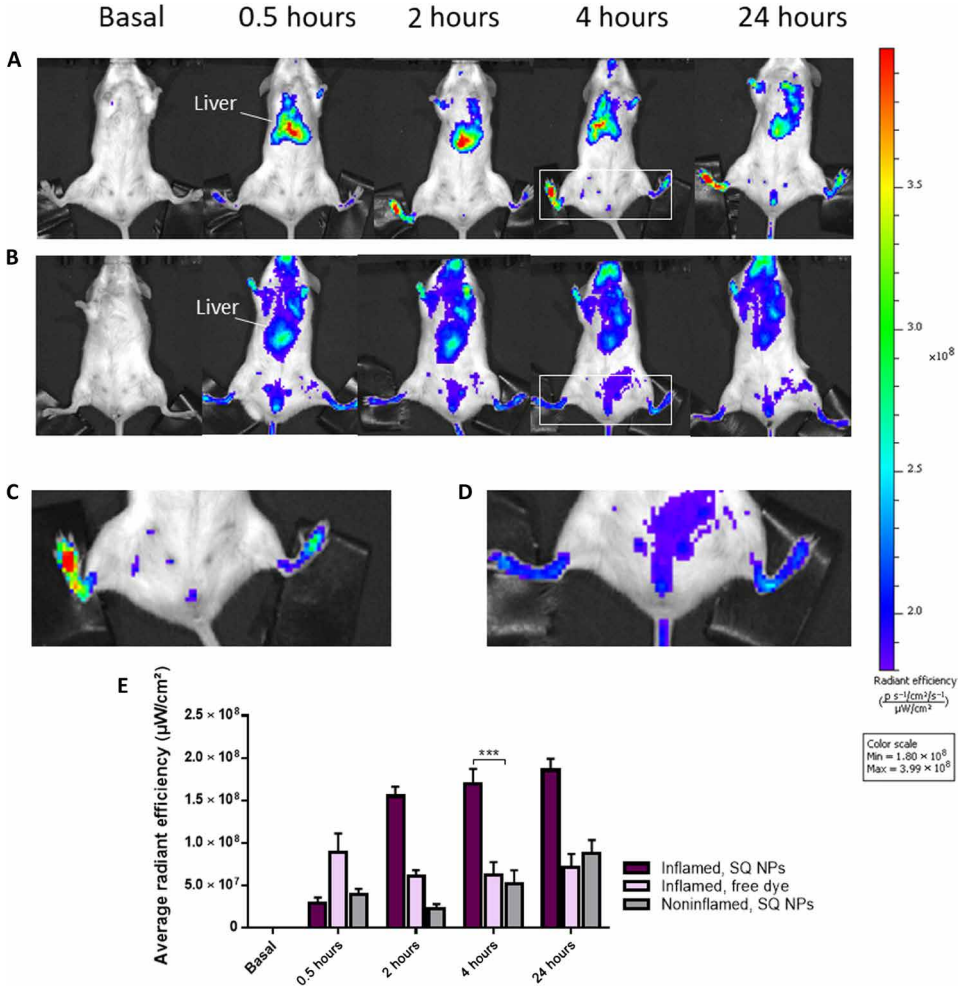

Fig. 2. IVIS Lumina scan of mice after intravenous administration of fluorescent SQAd/VitE NPs or control fluorescent dye solution (ventral view). (**A**) Tracking of fluorescent SQAd/VitE NPs in mice with inflamed right hind paw and noninflamed left hind paw. (**B**) Tracking of the free dye in mice with inflamed right hind paw. (**C**) Zoomed-in view of group A at 4 hours. (**D**) Zoomed-in view of group B at 4 hours. (**E**) Analysis of the measured total radiant efficiency in the region of interest. $n = 3$ mice per group. Data are mean ± SD. $^*P < 0.05$, $^{**}P < 0.01$, and $^{***}P < 0.001$ [two-way analysis of variance (ANOVA) followed by Tukey's multiple comparison test].

accumulation into the inflamed paw in comparison to PLGA NPs (fig. S3). A detailed discussion about this observation is provided in Supplementary Discussion.

In a second study, we evaluated the ability of SQAd/VitE NPs to accumulate in organs in a model of LPS-induced sepsis. Loss of endothelial integrity is one of the hallmarks of sepsis, and LPS injection has been shown to induce capillary leakage in a β1-integrin–dependent mechanism (*28*). Here, rhodamine B covalently linked to SQ (SQRho; figs. S1 and S2) was used as a fluorescent marker for SQAd/VitE NPs. Animals received LPS intraperitoneally and, after 2 hours, an intravenous injection of fluorescent SQAd/VitE NPs. After 24 hours, the mice were deeply anesthetized and intracardially perfused with 40 ml of phosphate-buffered saline (PBS) to remove blood. The fluorescence signal in the different organs was measured using an IVIS Lumina. Mice that did not receive an LPS challenge were used as noninflamed controls. The fluorescent imaging showed that, in comparison with healthy mice, LPS-inflamed animals had a significant increase in the levels of total radiant efficiency in the lungs, liver, and kidneys (Fig. 3). In a control experiment, when LPS-treated mice were intravenously injected with a free rhodamine probe solution, no significant accumulation occurred in the studied organs except the kidney, most probably because of the renal clearance of rhodamine.

During inflammation, neutrophils interact with the vascular endothelium leading to barrier dysfunction and increased permeability. This constitutes a unique opportunity for nanomedicines to accumulate at the sites of organ injury and selectively deliver therapeutic agents through enhanced permeation and retention effects (*29*). In the present in vivo studies, SQAd/VitE NPs were found to accumulate at the sites of acute inflammation and endothelial dysfunction in models of both local and systemic inflammation. When injected in vivo, free Ad is readily catabolized into inosine and hypoxanthine, resulting in an extremely short blood half-life of 10 s (*13*). This requires Ad to be administered continuously and in high doses to achieve a pharmacological response, resulting in side effects related to the unchecked activation of the ubiquitous Ad receptors. The targeted accumulation achieved by SQAd/VitE NPs could therefore potentially limit the side effects induced by Ad treatment and enhance the bioavailability of both drugs at the sites of inflammation for improved therapeutic action.

In vitro evaluation

To investigate whether SQAd/VitE NPs could effectively enact protection against oxidative stress, we first developed an in vitro model of oxidative insult. In inflamed tissue, immune cells produce ROS such as hydrogen peroxide (H_2O_2) that can cross the cellular membrane and produce intracellular oxidative stress (*30*) to tissue cells. When H9c2 murine cardiac cells were incubated with H_2O_2 for 30 min, a strong increase in intracellular ROS was detected by flow cytometry using a ROS-sensitive fluorescent probe. Treatment with SQAd/VitE NPs was efficient at limiting intracellular ROS production in a dose-dependent manner (Fig. 4, A and B). While SQAd NP and SQ NP controls did not provide this protection, free drug Ad/VitE in the medium did induce some protection against the oxidative insult, most probably because of the antioxidant action of VitE. This effect was less pronounced than with SQAd/VitE NPs. The reduction in intracellular ROS correlated positively with improved cell survival to the oxidative insult as measured by propidium iodide straining. In SQAd/VitE NP–treated samples, only 20% of cells were found to be necrotic, while nontreated cell populations contained 80% of necrotic cells (Fig. 4, C and D). SQAd/VitE NPs were found to be readily taken up by cells (fig. S5), likely through LDL receptor–mediated mechanisms as shown previously with SQAd-only NPs (*31*). Thus, after accumulating at the sites of inflammation, SQAd/VitE NPs are most likely able to enter cells, where they can deliver their therapeutic cargo intracellularly. As it has been suggested (*19*, *32*), and as demonstrated here, the intracellular delivery of the antioxidant VitE improved its capacity to diminish oxidative stress. This cellular uptake also likely allows SQAd/VitE NPs to generate the active Ad in a localized manner after hydrolysis of SQAd (*33*). It was previously observed that after LDL receptor–dependent internalization, the SQAd NPs located in endo-lysosomal compartments where they acted as intracellular reservoirs for the encapsulated Ad. Once the hydrolysis of the amide bond released Ad, equilibrative nucleoside transporters (ENTs) discharged the drug Ad outside of the cell where it interacted with Ad receptors (*32*).

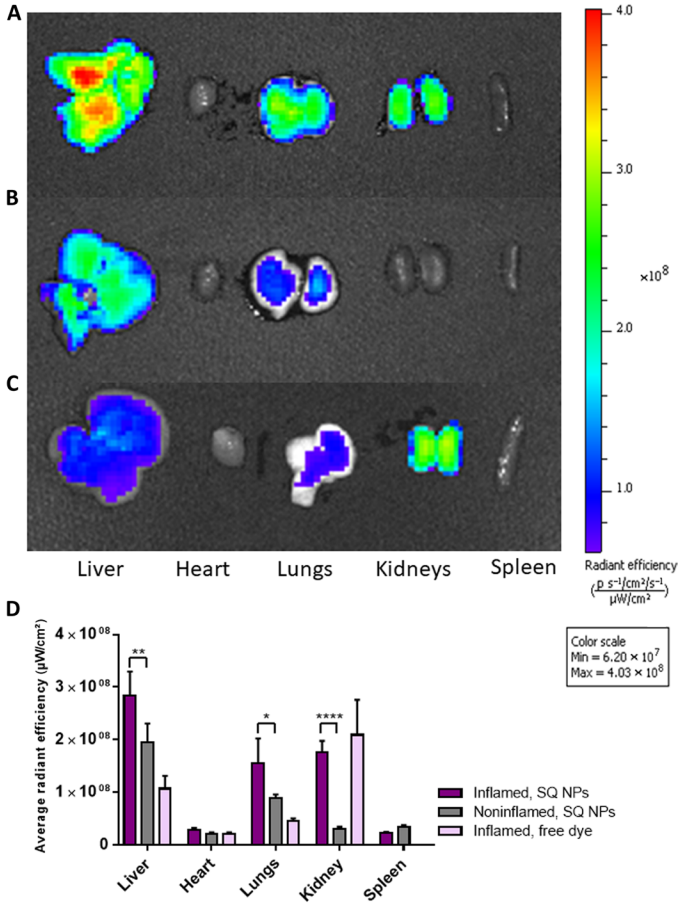

Fig. 3. Ex vivo IVIS Lumina scan of mice organs after intravenous administration of fluorescent SQAd/VitE NPs in a septic shock model. Organs displayed from left to right: liver, heart, lungs, kidneys, and spleen. (**A**) Tracking of fluorescent SQAd/VitE NPs labeled in mice that received a LPS challenge. (**B**) Tracking of fluorescent SQAd/VitE NPs in noninflamed mice (did not receive LPS challenge). (**C**) Tracking of free dye in mice that received a LPS challenge. (**D**) Analysis of the measured total radiant efficiency in the different organs. $n = 3$ mice per group. Data are mean ± SD. $^*P < 0.05$, $^{**}P < 0.01$, and $^{****}P < 0.0001$ (two-way ANOVA followed by Tukey's multiple comparison test).

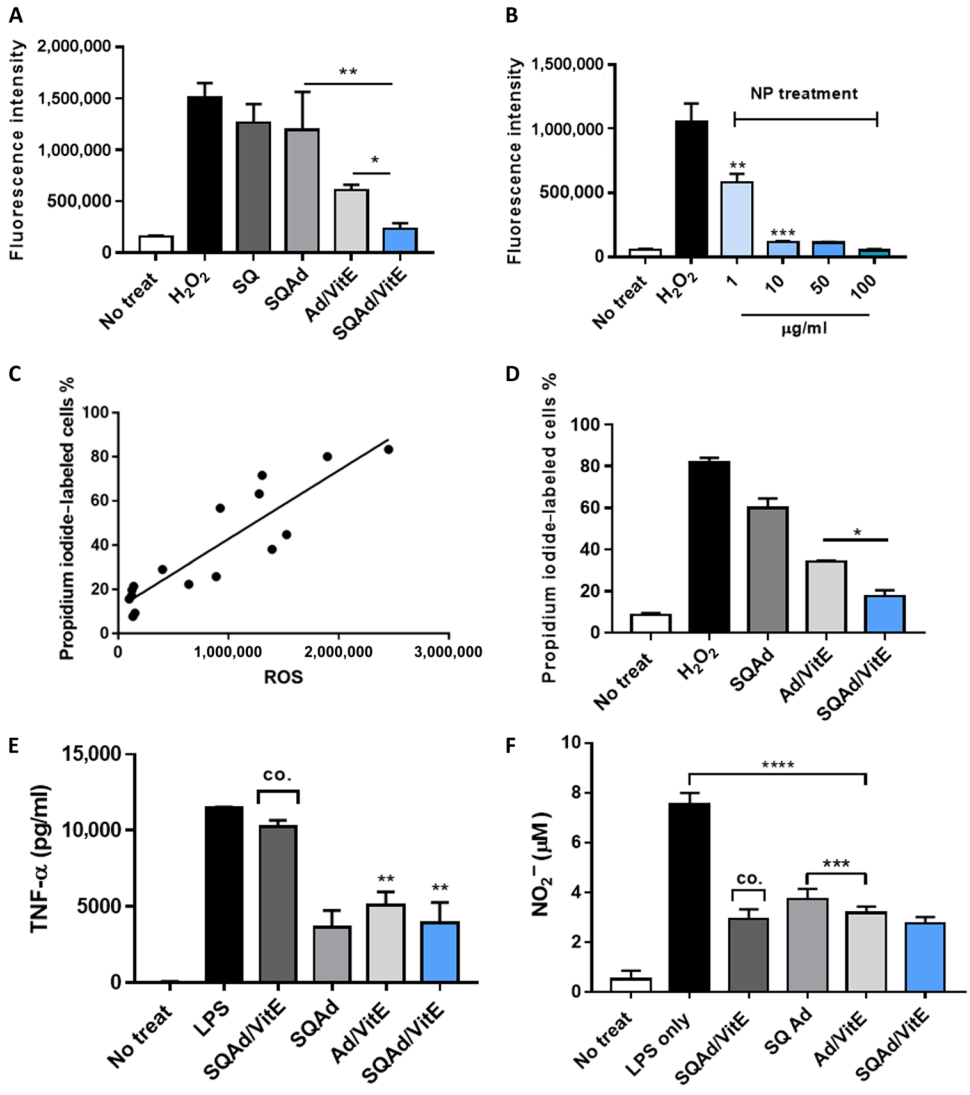

Fig. 4. In vitro antioxidant and anti-inflammatory properties of SQAd/VitE NPs. (**A**) Fluorescent detection of ROS in H9c2 cells showing that SQAd/VitE NPs efficiently scavenge intracellular ROS compared to free-drug or single-drug controls. (**B**) Dose dependence of the ROS protective effect of SQAd/VitE NPs on H9c2 cells. (**C**) Correlation of necrotic cell death with the amount of detected intracellular ROS. (**D**) Evaluation of necrotic cell death by propidium iodide staining. (**E**) Quantification of pro-inflammatory cytokine TNF-α production in LPS-stimulated RAW 264.7 cells treated with SQAd/VitE NPs or controls. co. SQAd/VitE NP treatment concurrently to LPS challenge. (**F**) Evaluation of nitrite content in cell medium following LPS stimulation of RAW 264.7 macrophages with or without SQAd/VitE NP treatment and controls. Data are the mean ± SD. $n = 3$ independent experiments. *$P < 0.05$, **$P < 0.01$, ***$P < 0.001$, and ****$P < 0.0001$ (one-way ANOVA followed by Holm-Sidak's multiple comparison test).

We next evaluated the ability of SQAd/VitE NPs to efficiently inhibit pro-inflammatory signaling. For this, RAW 264.7 macrophages were used in an in vitro LPS-induced inflammation model. RAW macrophages respond to LPS stimulation by releasing pro-inflammatory cytokines (*34*). Accordingly, when RAW macrophages were stimulated with LPS (1 µg/ml), a significant increase in tumor necrosis factor–α (TNF-α) cytokine was measured in the supernatant. This pro-inflammatory response was inhibited by treatment with SQAd/VitE NPs at a concentration of 10 µg/ml for 2 hours. Here, SQAd and SQAd/VitE NPs had similar effects on the release of inflammatory cytokines, indicating that Ad could be the main effector of the observed anti-inflammatory effect (Fig. 4E). When SQAd/VitE treatment was performed simultaneously to the LPS challenge, no significant inhibition of pro-inflammatory signaling was observed, contrary to free drug Ad/VitE. This substantiated the idea that SQAd is not active as an anti-inflammatory agent but needs to be activated in situ to perform anti-inflammatory activity (*33*).

LPS stimulation of macrophages also causes overproduction of nitric oxide by inducible nitric oxide synthase (iNOS) (*35*), which results in further pro-inflammatory signaling and oxidative stress by reactive nitrogen species (NOx) (*36*). Thus, RAW 264.7 macrophages were stimulated with LPS, and nitrite accumulation was monitored by Griess reagent to evaluate the consequence of SQAd/VitE NP treatment on NOx formation. Stimulation by LPS (1 µg/ml) resulted in 7.5 µM nitrite content in the supernatant, but NOx production was significantly inhibited after incubation of SQAd/VitE NPs at 10 µg/ml (Fig. 4F). Free drugs Ad/VitE controls also showed efficient inhibition of nitrite accumulation, which likely resulted from free Ad, acting on its cognate receptors A2A and A2B, inhibiting iNOS expression (*37*, *38*). Here, there was no difference in the SQAd/VitE

groups between pretreated cells or cells simultaneously treated with NPs at the time of LPS challenge (see also Supplementary Discussion). Noteworthy, nitrite production was significantly lower in SQAd/VitE NP–treated cells compared to cells that only received SQAd. This showed that increasing drug loading through the use of prodrug-based nanocarriers might be advantageous for inflammation therapy.

Overall, these results showed that multidrug SQAd/VitE NPs could effectively scavenge ROS in a concentration-dependent manner and established effective proresolving action through the combined effects of SQAd and VitE in vitro. By using a prodrug-based nanoformulation, SQAd/VitE NPs did not trigger Ad signaling until Ad release, which could limit deleterious side effects associated with Ad therapy.

In vivo efficacy of SQAd/VitE NPs in endotoxemia model

We then proceeded to evaluate the in vivo ability of SQAd/VitE NPs to promote the resolution of inflammation in mice by examining their effect on the acute inflammatory response to endotoxin. In the blood, recognition of LPS by circulating macrophages activates the redox-controlled nuclear factor κB (NF-κB) by Toll-like receptor 4 (TLR4)–mediated mechanisms. This event potentiates downstream inflammation cascades, resulting in the pathological "cytokine storm." In our experiments, LPS was injected in mice intraperitoneally, after which blood and organs were collected at various time points to measure the levels of pro-inflammatory and anti-inflammatory cytokines by enzyme-linked immunosorbent assay (ELISA). In the blood, pro-inflammatory cytokine levels reached a maximum 1 hour after the LPS challenge, while anti-inflammatory cytokines followed with a peak 2 hours after LPS injection (fig. S6). In the treatment group where SQAd/VitE NPs were injected at a dose of 30 mg/kg [corresponding to Ad (5.5 mg/kg) and VitE (15 mg/kg)], a significant decrease in TNF-α together with an increase in anti-inflammatory interleukin-10 (IL-10) could be observed, comparatively to control groups that received either no treatment, free drugs Ad/VitE, SQAd NPs, or SQVitE NPs only at equivalent doses (Fig. 5, A and B). This effect took place in a dose-dependent manner (fig. S7). Free drug Ad and VitE have limited bioavailability due to extremely fast metabolization and poor cell localization, respectively. These initial in vivo results pointed to an improved pharmacological profile of these compounds, thanks to their formulation as NPs and protection from early degradation.

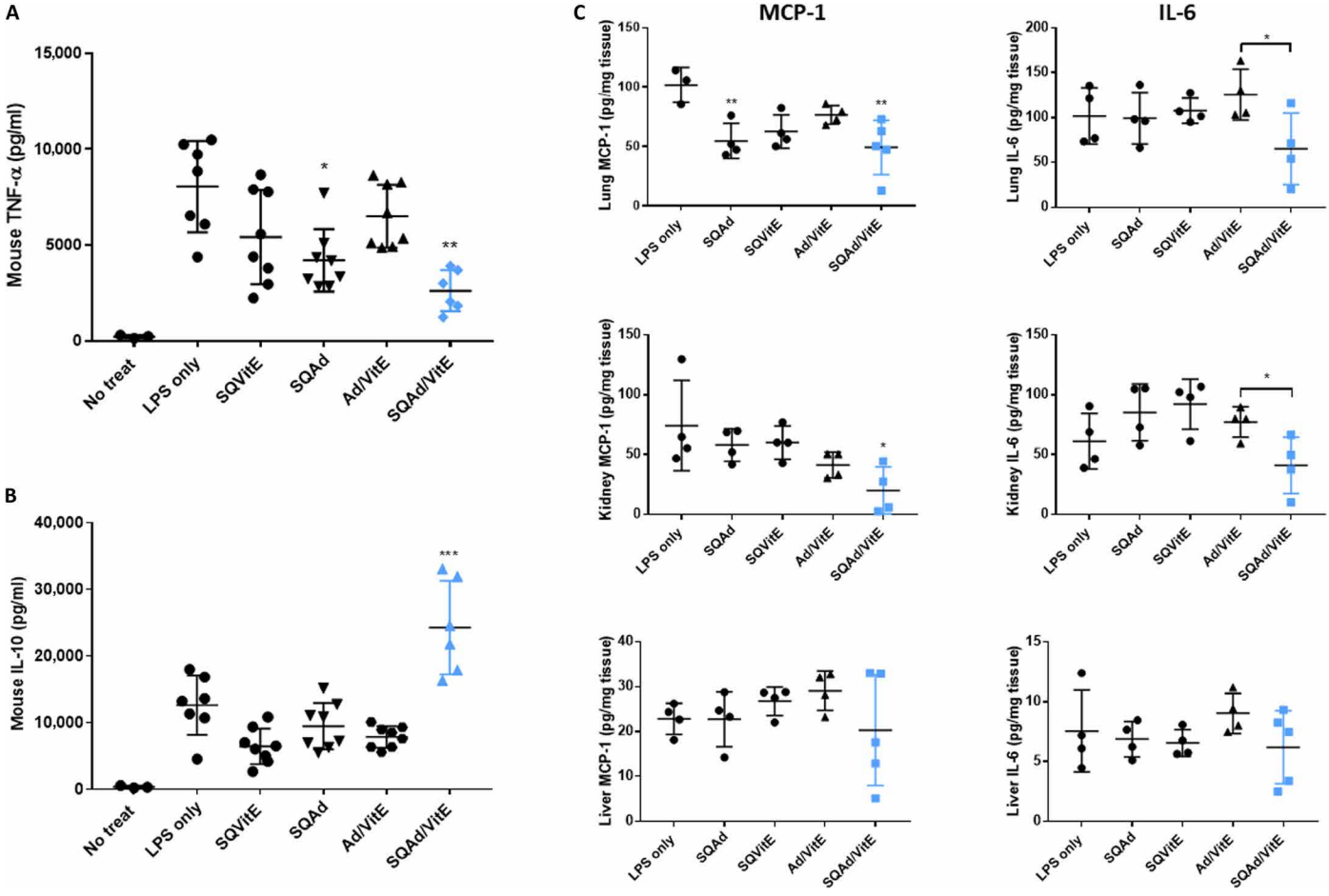

Fig. 5. In vivo influence of SQAd/VitE NPs on inflammatory cytokines. (**A**) Mouse TNF-α in plasma 1 hour after LPS challenge as measured by ELISA. (**B**) Mouse IL-10 in plasma 1 hour after LPS challenge as measured by ELISA. (**C**) Pro-inflammatory cytokines including MCP-1 and IL-6 from the lungs, liver, and kidneys, 4 hours after LPS challenge as measured by cytometric bead array. Nontreated controls did not reach detection threshold and were not shown. $n = 4$ to 8 mice per group. Data are mean ± SD. ns, not significant; $^{*}P < 0.05$, $^{**}P < 0.01$, and $^{***}P < 0.001$ significant difference to LPS only control unless specified (one-way ANOVA followed by Holm-Sidak's multiple comparison test).

Next, we evaluated in organ homogenates the levels of two key pro-inflammatory cytokines MCP-1 (monocyte chemoattractant protein-1) and IL-6, responsible, respectively, for recruiting immune cells to the sites of inflammation and mediating the acute-phase response (*39*). In the lungs and kidneys, 4 hours after the initial LPS challenge, treatment with SQAd/VitE NPs at 30 mg/kg significantly reduced the amount of MCP-1 and IL-6 compared to nontreated or free drug–treated controls (Fig. 5C). In the liver, results failed to reach significance, but a tendency for mitigated acute inflammation could be observed.

We next evaluated the antioxidant effects of SQAd/VitE NPs in vivo by measuring the amount of lipid peroxidation products in the lungs following the LPS challenge. During acute systemic inflammation, the immune cells recruited by the extensive pulmonary capillary bed induce high levels of oxidative stress in the lungs, resulting in substantial lipid peroxidation (*40*). LPS challenge resulted in an increase in lipid peroxidation products as measured by reaction of malondialdehyde (MDA) with thiobarbituric acid reactive substance (TBARS test) (5.5 nmol of MDA/mg protein versus 2.75 nmol of MDA/mg protein). Basal MDA levels in mice typically range around 2 nmol of MDA/mg protein (*41*–*43*). Although it could not be abrogated, the increase in MDA was most strongly mitigated in the SQAd/VitE NP treatment group, where MDA levels reached only 4.04 nmol of MDA/mg protein (Fig. 6A).

Together, these in vivo studies demonstrated an efficient and targeted resolution of inflammation by multidrug SQAd/VitE NPs. While single-drug NPs did display some efficacy at inhibiting plasma TNF-α, they did not reach the therapeutic efficacy of SQAd/VitE NPs. Contrary to what was observed in in vitro studies, in vivo free drug Ad/VitE controls consistently failed to induce a significant therapeutic response. This could be explained by the quick metabolization of Ad after a bolus injection (*44*) and poor bioavailability of VitE. Our prodrug-based NPs thus increased the efficacy of both drugs by simultaneously delivering them to the sites of inflammation.

Side effects on healthy animals and efficacy in lethal LPS model

To further validate the in vivo capability of SQAd/VitE NPs, we then investigated the hemodynamic effects of SQAd/VitE NPs comparatively to free drugs Ad/VitE. The effects of a single injection of SQAd/VitE NPs on blood pressure were measured noninvasively on healthy mice. While the NP-encapsulated drugs had no significant effect on blood pressure compared to nontreated controls, free drugs Ad/VitE induced a measurable decrease in blood pressure due to Ad, in accordance with published literature (Fig. 6B) (*45*). These results confirmed that the SQAd/VitE NP formulation helped to protect animals from the deleterious side effects induced by Ad therapy.

We therefore proceeded to evaluate the efficacy of SQAd/VitE NPs in a model of lethal LPS challenge (*46*). Mice in the treatment groups received either SQAd/VitE NPs at a dose of 30 mg/kg or free drugs Ad/VitE at an equivalent dose. In the group treated with SQAd/VitE NPs, all mice survived the lethal LPS challenge, whereas free drug Ad/VitE failed to significantly improve the survival rate, compared to the untreated control animals (Fig. 6D). Improvements in the clinical scores of the animals paralleled the improvements in survival rates for all groups (Fig. 6C). Last, the consequence of the treatment with SQAd/VitE NPs was histologically investigated regarding signs of inflammation. In the previous LPS lethality model, organs from either SQAd/VitE NP–treated mice or LPS only–treated

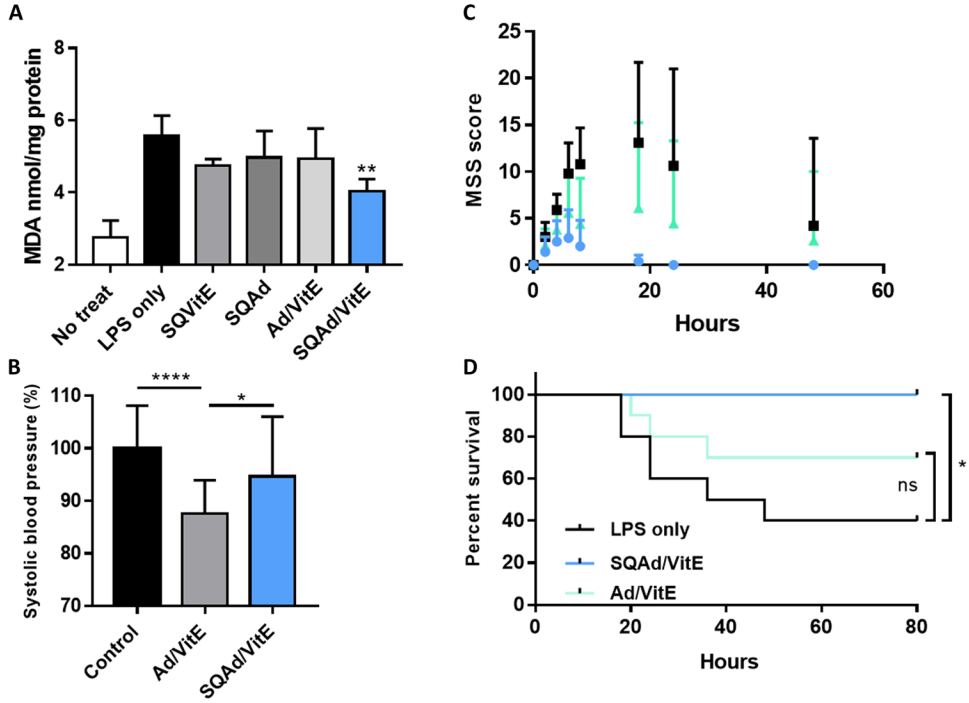

Fig. 6. In vivo therapeutic efficacy of SQAd/VitE NPs in endotoxemia models. (**A**) Level of lipid peroxidation in the lungs as measured by TBARS quantification of MDA. $n = 3$ mice per group. (**B**) Systolic blood pressure determination as % of control in healthy animals following SQAd/VitE or Ad/VitE treatment. $n = 3$ animals per group, five measurements per animal. (**C**) MSS (murine sepsis score) clinical score of animals undergoing LPS endotoxemic shock. $n = 10$ mice per group. (**D**) Survival followed after lethal LPS injection for 80 hours. $n = 10$ mice per group. Data are the mean ± SD. $^{*}P < 0.05$, $^{**}P < 0.01$, and $^{***}P < 0.001$ significant difference to LPS only control unless specified (one-way ANOVA followed by Holm-Sidak's multiple comparison test). For survival evaluation, a log-rank (Mantel-Cox) test was used, giving a $P = 0.0130$.

controls were harvested at the 24-hour point and analyzed for histological signs of tissue stress following hematoxylin and eosin (H&E) staining. Inflammatory changes including mononuclear cell infiltration, endothelial disruption, and hemorrhage were noticeably reduced in animals that received SQAd/VitE NP treatment. In the liver, nontreated animals displayed severe injuries, which were not observed in SQAd/VitE NP–treated animals (figs. S8 and S9); these included hemorrhagic sinusal occlusion, advanced hepatocellular stress, and disseminated steatosis. In the lungs, although both animal groups showed signs of inflammatory stress, the nontreated animals displayed more advanced loss of structure, alveolar thickening, and hemorrhage (fig. S9).

As is the case with many animal models, lethal endotoxemia sepsis models, although widely used to study anti-inflammatory therapies (*47*–*49*), have inherent drawbacks. The main limitation of this model is the speed at which it induces a severe inflammatory insult. Numerous studies have investigated therapeutic compounds in the context of sepsis by pretreating animals before LPS injection (*50*, *51*). Other studies investigated treatment at the time of LPS injection (*52*). In clinical practice, patients with sepsis usually receive treatment after the onset of the pro-inflammatory insult but before the insult reaches "peak severity." In this endotoxemia model, we found that pro-inflammatory cytokines such as TNF-α reached a maximum about 1 hour after LPS injection (see fig. S6). As a result, we decided to inject our treatments at the 30-min time point, halfway between the onset and the peak of the inflammatory response, which is probably the best time point to fit with the clinical conditions.

CONCLUSION

We presented here the first example of targeted delivery of Ad, and of multidrug anti-inflammatory/antioxidant NPs, for the mitigation of inflammation. Bioconjugation of Ad to SQ allowed to obtain a prodrug-based nanocarrier, which, after nanoformulation with VitE, yielded stable multidrug NPs, improving the bioavailability of both drugs with significant pharmaceutical activity in models of acute inflammatory injury. With the ability to specifically target and deliver Ad at tissue foci of acute inflammation and the capacity to react with intracellular reactive species at the target site, SQAd/VitE NPs represent a promising therapeutic intervention overcoming limitations of both conventional Ad and antioxidant therapy. Our extensive in vivo data support this hypothesis that opens the way to explore the plethora of available specific Ad receptor agonists and antioxidants. Additional efforts will also allow to further characterize SQ-based NP biodistribution. Overall, these SQ-based multidrug NPs represent a unique approach for inhibiting the pathological cross-talk between oxidative stress and inflammation, delivering therapeutic agents at the loci of inflammation, and thus afford a new tool in the fight against the complex and multifactorial phenomenon of uncontrolled inflammation.

MATERIALS AND METHODS

Preparation of SQ-based NPs

SQAd was synthesized as previously described (*25*), and the resulting NPs were prepared using the nanoprecipitation technique. Briefly, SQAd was dissolved in absolute ethanol (6 mg/ml) and added dropwise under strong stirring to a 5% (w/v) dextrose solution. Ethanol was then completely evaporated using a Rotavapor (90 rpm, 40°C, 42 mbar) to obtain an aqueous suspension of pure SQAd NPs (2 mg/ml). Multidrug SQAd/VitE NPs (50:50 wt %) were obtained by dissolving SQAd (3 mg/ml) and VitE (3 mg/ml) (α-tocopherol, Sigma-Aldrich) in absolute ethanol and adding the solution dropwise under strong stirring to a 5% dextrose solution with subsequent ethanol evaporation to obtain an aqueous suspension of SQAd/VitE NPs (2 mg/ml). Fluorescent NPs were obtained by the same procedure, except 1% (w/w) of fluorescent probe (SQRho) or DiD perchlorate (Thermo Fisher Scientific) was added to the ethanolic phase. All NP sizes (hydrodynamic diameter) and surface charges (zeta potential) were measured using a Malvern Zetasizer Nano ZS 6.12 (173° scattering angle, 25°C). For the size measurements by DLS, a good attenuator value (*7*–*9*) was obtained when suspending 20 μl of NPs in 1 ml of distilled water. The mean diameter for each preparation resulted from the average of three measurements of 60 s each. For zeta potential measurements, 70 μl of NPs was dissolved in 2 ml of 1 mM KCl before filling the measurement cell. The mean zeta potential for each preparation resulted from the average of three independent measurements in automatic mode, followed by application of the Smoluchowski equation. Morphology was observed by cryo-TEM. For this, drops of the NP suspensions (2 mg/ml) were deposited on electron microscopy grids covered with a holey carbon film (Quantifoil R2/2) previously treated with a plasma glow discharge. Observations were conducted at low temperature (−180°C) on a JEOL 2010 field emission gun microscope operated at 200 kV. Images were recorded with a Gatan camera.

Encapsulation efficiency experiment

SQAd/VitE NPs with different VitE content were formulated in 5% dextrose solution and subsequently washed with water twice using an ultrafiltration device (molecular weight cutoff, 100,000). NPs were dissolved in ethanol and measured by HPLC to determine VitE content. HPLC Waters Alliance 1695 (Waters, Milford, MA), equipped with a Waters DAD 2996 photodiode array detector, Hewlett-Packard computer with a Waters Empower 3 software, and a Waters autosampler with a 50-μl loop, was used, with simultaneous spectra detection wavelengths from 200 to 600 nm recorded for all peaks. A Waters XSelect LC-18 column (2.1 mm by 150 mm, 3.5 μm) was used with a nongradient mobile phase of acetonitrile and methanol (50:50, v/v) at a constant flow rate of 1 ml/min. The VitE peak was measured at a wavelength of 216 nm and quantitatively determined by comparing with a standard curve.

In vitro release of Ad from NPs in serum

Fetal bovine serum (3 ml) was prepared with 172 μl of EHNA (erythro-9-(2-hydroxy-3-nonyl)adenine) [Ad deaminase inhibitor (1 mg/ml), NaCl 0.9%; Sigma-Aldrich] and 4.8 μl of dipyridamole [Ad uptake inhibitor (30 mg/ml), dimethyl sulfoxide; Sigma-Aldrich]. SQAd/VitE NPs (180 μl; 2 mg/ml) were incubated at different time intervals with 180 μl of the fetal bovine serum solution in various Eppendorf vials, each for one time point. At the predetermined time intervals (i.e., 5 min, 30 min, 2 hours, 15 hours, 24 hours, and 48 hours), aliquots (100 μl) were collected and added into 500 μl of MeOH to denature and precipitate the enzymes and proteins of the serum, which were removed after centrifugation (16,000*g* for 10 min). To quantify the remaining SQAd bioconjugate and the released Ad, the remaining supernatants (150 μl) were evaporated to dryness at 40°C under nitrogen flow and then solubilized in 100 μl of MeOH. Quantification was performed using a reversed-phase HPLC on a Halo C18 column (4.6 mm by 250 mm, 5 μm; Interchim), a 1525

Binary LC Pump (Waters), a 2707 Autosampler (Waters), and a 2998 PDA detector (Waters). The HPLC was carried out using a gradient elution with the mobile phase composed of 80% 10 mM potassium phosphate in Milli-Q water (pH 4.0) 20% MeOH (phase A) and MeOH (phase B). Elution was carried out at a flow rate of 0.8 ml/min. The system was held at 100% of A for 8 min, followed by 1-min linear gradient from 100% A to 100% B, kept at 100% B for 12 min, and brought back to initial condition by a 1-min linear gradient from 100% B to 100% A. The sample run was maintained for 7 min with 100% A to equilibrate the column pressure. Temperature was set at 30°C, and ultraviolet detection was monitored at 260 nm for Ad and 272 nm for SQAd. The detection limit of the HPLC technique was 2 μg/ml for Ad and 10 μg/ml for SQAd. This method exhibited linearity (R^2 = 0.9988) over the assayed concentration ranges (2 to 200 μg/ml).

Intracellular ROS detection assay

H9c2 cells (50,000 cells per well) were seeded in a 12-well plate and cultured for 24 hours at 37°C. The cells were treated for 2 hours with SQAd/VitE NPs or controls diluted in culture medium at a concentration of 10 μg/ml for standard tests or according to the described dose for dose-response experiments. Cells were washed with PBS and incubated with medium containing hydrogen peroxide (H_2O_2; final concentration, 0.5 mM; Sigma-Aldrich). After 30 min, H_2O_2-containing medium was removed, and the cells were washed with PBS. Intracellular ROS production was detected using Abcam Cellular ROS Assay Kit (Deep Red) per manufacturer's instructions. Briefly, the ROS detection probe was diluted in PBS, and cells were incubated with this staining solution for 30 min. Staining solution was removed, and cells were washed with PBS and treated with 300 μl of 0.25% trypsin solution for 5 min at 37°C. The trypsin solution was inhibited by adding 0.7 ml of medium, and cell fluorescence was recorded using an Accuri flow cytometer C6 (Accuri Cytometers Ltd.). Necrotic cell death was assessed by propidium iodide staining at 10 μg/ml.

Nitric oxide assay

Nitrite (NO_2^-) release was assessed with freshly prepared Griess reagent. Briefly, in 96-well plates (20,000 cells per well), RAW 264.7 cells were treated for 2 hours with SQAd/VitE NPs or controls diluted in culture medium at a concentration of 10 μg/ml. LPS (Sigma-Aldrich O111:B4) was added at a final concentration of 1 μg/ml for 24 hours for macrophage stimulation. For co-treatment experiments, SQAd/VitE NP treatment was also performed concurrently to LPS stimulation. After LPS stimulation, the Griess reagent was added in equal volume to culture supernatants. The absorbance at 550 nm was measured on a PerkinElmer absorbance reader after 10 min of incubation in the dark at room temperature. The NO_2^- concentrations were determined using standard curves prepared from sodium nitrite ($NaNO_2$) at various concentrations.

In vitro evaluation of pro-inflammatory cytokine production

LPS stimulation and drug treatments were performed in the same way than with nitric oxide assays. After LPS stimulation for 24 hours, cell supernatants were retrieved and centrifuged for 5 min at 1000*g* to remove cell debris. Inflammatory cytokine production was evaluated using a BioLegend ELISA mouse TNF-α cytokine detection kit per manufacturer's instructions (BioLegend, USA). Supernatants were diluted 20× with Assay Diluent before detection experiment.

Animal care

Male C57BL/6J and female BALB/c mice were purchased from Janvier Labs (France) for systemic inflammation and NP tracking studies, respectively. Animals were housed in a standard controlled environment (22° ± 1°C, 60% relative humidity, 12-hour light/dark cycles) with food and water available ad libitum. Experiments were approved by the Animal Care Committee of the University Paris-Sud, in accordance with the principles of laboratory animal care and European legislation 2010/63/EU. All efforts were made to reduce animal numbers and minimize their suffering, as defined in the specific agreement (registration no. APAFIS#16257).

NP tracking studies

For the paw inflammation study, experiments were performed on 18-week-old female BALB/c mice. Paw inflammation was caused by intraplantar injection in the right paw of 100 ng of LPS (Sigma-Aldrich O111:B4) dissolved at 5 mg/ml in physiological saline (NaCl, 0.9%). Animals received a control injection of 20 μl of saline in the left paw. In vivo imaging studies were performed after 2 hours, following intravenous injection of fluorescent SQAd/VitE or PLGA NPs (100 μl, 2 mg/ml, containing 1% DiD) or control fluorescent DiD solution (100 μl, 20 μg/ml in 5% dextrose solution). The biodistribution of the NPs was recorded at 0.5, 2, 4, and 24 hours with the IVIS Lumina LT Series III system (Caliper Life Sciences) using 640-nm excitation and 695-nm emission filters. During imaging, mice were kept on the imaging stage under anesthesia with 2% isofluorane gas in oxygen flow (1 liter/min) and were imaged in ventral position. Images and measures of fluorescence signals were acquired and analyzed with Living Imaging software (Caliper Life Sciences).

For the systemic inflammation study, experiments were performed on 12-week-old male C57BL/6J mice. Systemic inflammation was caused by intraperitoneal injection of LPS (Sigma-Aldrich O111:B4) at a dose of 7.5 mg/kg. Noninflamed control animals did not receive the LPS injection. After 2 hours, animals received intravenous injection of fluorescent SQAd/VitE NPs (100 μl, 2 mg/ml, containing 1% SQRho) or control fluorescent rhodamine B solution (100 μl, 20 μg/ml in 5% dextrose solution). After 24 hours, animals were deeply anesthetized with an intraperitoneal sodium pentobarbital injection before euthanasia by intracardial perfusion of 40 ml of saline (8 ml/min), until the fluid exiting the right atrium was entirely clear. The liver, heart, lungs, kidneys, and spleen were excised and immediately imaged with the IVIS imager using 560-nm excitation and 620-nm emission filters. Images and measures of fluorescence signals were acquired and analyzed with Living Imaging software (Caliper Life Sciences).

In vivo efficacy

The therapeutic efficacy of SQAd/VitE NPs was evaluated in vivo in a mouse endotoxemia model with 8- to 12-week-old male C57BL/6J mice. To evaluate the efficacy through cytokine production, endotoxemia was induced by intraperitoneal injection of a dose of LPS (7.5 mg/kg; Sigma O111:B4) diluted at 1.875 mg/ml in buffered saline. Mice injected with LPS alone were used as controls. Thirty minutes after LPS injection, SQAd/VitE NPs [SQAd (15 mg/kg), i.e., Ad (equivalent 5.5 mg/kg) and VitE (15 mg/kg)], SQAd NPs [SQAd (15 mg/kg) and Ad (equivalent 5.5 mg/kg)], or free Ad/VitE [Ad (5.5 mg/kg) and VitE (15 mg/kg) with 1% Pluronic F-123 vehicle for VitE solubilization] were intravenously injected via the suborbital vein. Following the injections, blood samples (~100 μl) were collected at

predetermined time points via submandibular puncture before terminal cardiac puncture and organ collection. Plasma was obtained by centrifuging blood samples at 2000 rcf (relative centrifugal force) for 10 min and stored at −78°C before further analysis. In the plasma, cytokines, including IL-10 and TNF-α, were quantified by BioLegend ELISA mouse kit per manufacturer's instructions. Organ homogenates were obtained with a Heidolph Instruments (Germany) RZR-2021 organ homogenizer in PBS at a concentration of 500 mg/ml. Pro-inflammatory cytokines in organ homogenates were quantified using a cytometric bead array per manufacturer's instruction (BD Biosciences). For MDA content in the lungs, 10 mg of lung tissues was homogenized on ice in 300 µl of MDA lysis buffer containing 3 µl of BHT (butylated hydroxytoluene) antioxidant solution as per manufacturer's instruction (Biovision, Lipid Peroxidation MDA Fluorometric Assay Kit). To evaluate efficacy through survival in the lethal LPS model, mice were sensitized to the lethal effects of LPS with D-galactosamine hydrochloride (Roth, Germany) via intraperitoneal injection of an 8-mg dose concurrently to LPS injection at 2 µg/kg. After 30 min, NPs or free drugs as controls were injected intravenously. Signs of disease severity were evaluated at predetermined time points using a previously described disease scoring system (*53*). For histological evaluation, organs were fixed for 24 hours in 4% paraformaldehyde and then embedded in paraffin. Sections (5 µm) were deparaffinized and stained with H&E (VWR, France). Slides were scanned with a digital slide scanner NanoZoomer 2.0-RS (Hamamatsu, Japan), which allowed an overall view of the samples. Images were digitally captured from the scan slides using the NDP.view2 software (Hamamatsu).

Blood pressure measurements

For blood pressure measurements, a Kent Scientific (Torrington, USA) Coda tail-cuff VPR blood pressure measurement system was used. C57BL/6J mice were acclimated to the procedure for 2 days before measurements to avoid undue stress and experimental artifact. For all measurements, an experimental session of 10 acclimation cycles and 10 measurement cycles was used. Only measurement cycles that passed Coda software acceptance criteria were retained. For animals that received free drug Ad/VitE or SQAd/VitE (30 mg/kg or equivalent), the blood pressure measurement was started immediately after intravenous injection.

Statistics

Statistics were computed with GraphPad Prism 6. Differences in group means were calculated by one-way analysis of variance (ANOVA) followed by Holm-Sidak's multiple comparison test or Kruskal-Wallis test (nonparametric) followed by Dunn's multiple comparison test when samples failed equality of variance or normality statistical tests (Shapiro-Wilk). A value of $P < 0.05$ was considered significant. For studies requiring grouped analyses, a two-way ANOVA followed by Tukey's multiple comparison test was performed.

SUPPLEMENTARY MATERIALS

Supplementary material for this article is available at http://advances.sciencemag.org/cgi/content/full/6/23/eaaz5466/DC1

View/request a protocol for this paper from *Bio-protocol*.

REFERENCES AND NOTES

1. H. Gomez, C. Ince, D. De Backer, P. Pickkers, D. Payen, J. Hotchkiss, J. A. Kellum, A unified theory of sepsis-induced acute kidney injury: Inflammation, microcirculatory dysfunction, bioenergetics and the tubular cell adaptation to injury. *Shock* **41**, 3–11 (2014).
2. F. Dormont, M. Varna, P. Couvreur, Nanoplumbers: Biomaterials to fight cardiovascular diseases. *Mater. Today* **21**, 122–143 (2018).
3. R. B. Goodman, J. Pugin, J. S. Lee, M. A. Matthay, Cytokine-mediated inflammation in acute lung injury. *Cytokine Growth Factor Rev.* **14**, 523–535 (2003).
4. P. Mehta, D. F. McAuley, M. Brown, E. Sanchez, R. S. Tattersall, J. J. Manson, COVID-19: Consider cytokine storm syndromes and immunosuppression. *The Lancet* **395**, 1033–1034 (2020).
5. T. van der Poll, F. L. van de Veerdonk, B. P. Scicluna, M. G. Netea, The immunopathology of sepsis and potential therapeutic targets. *Nat. Rev. Immunol.* **17**, 407–420 (2017).
6. C. A. Prauchner, Oxidative stress in sepsis: Pathophysiological implications justifying antioxidant co-therapy. *Burns* **43**, 471–485 (2017).
7. S. K. Biswas, Does the interdependence between oxidative stress and inflammation explain the antioxidant paradox? *Oxid. Med. Cell. Longev.* **2016**, 5698931 (2016).
8. J. Lugrin, N. Rosenblatt-Velin, R. Parapanov, L. Liaudet, The role of oxidative stress during inflammatory processes. *Biol. Chem.* **395**, 203–230 (2014).
9. A. Dandekar, R. Mendez, K. Zhang, *Stress Responses* (Springer, 2015), pp. 205–214.
10. B. Gibbison, J. A. López-López, J. P. Higgins, T. Miller, G. D. Angelini, S. L. Lightman, D. Annane, Corticosteroids in septic shock: A systematic review and network meta-analysis. *Crit. Care* **21**, 78 (2017).
11. B. N. Cronstein, G. Haskó, Regulation of inflammation by adenosine. *Front. Immunol.* **4**, 85 (2013).
12. G. Haskó, C. Szabó, Z. H. Németh, V. Kvetan, S. Pastores, E. S. Vizi, Adenosine receptor agonists differentially regulate IL-10, TNF-α, and nitric oxide production in RAW 264.7 macrophages and in endotoxemic mice. *J. Immunol.* **157**, 4634–4640 (1996).
13. U. Söderbäck, A. Sollevi, B. Fredholm, The disappearance of adenosine from blood and platelet suspension in relation to the platelet cyclic AMP content. *Acta Physiol. Scand.* **129**, 189–194 (1987).
14. L. Belardinelli, J. Linden, R. M. Berne, The cardiac effects of adenosine. *Prog. Cardiovasc. Dis.* **32**, 73–97 (1989).
15. G. Haskó, J. Linden, B. Cronstein, P. Pacher, Adenosine receptors: Therapeutic aspects for inflammatory and immune diseases. *Nat. Rev. Drug Discov.* **7**, 759–770 (2008).
16. H. Mangge, K. Becker, D. Fuchs, J. M. Gostner, Antioxidants, inflammation and cardiovascular disease. *World J. Cardiol.* **6**, 462–477 (2014).
17. M. M. Berger, R. L. Chioléro, Antioxidant supplementation in sepsis and systemic inflammatory response syndrome. *Crit. Care Med.* **35**, S584–S590 (2007).
18. E. Borrelli, P. Roux-Lombard, G. E. Grau, E. Girardin, B. Ricou, J.-M. Dayer, P. M. Suter, Plasma concentrations of cytokines, their soluble receptors, and antioxidant vitamins can predict the development of multiple organ failure in patients at risk. *Crit. Care Med.* **24**, 392–397 (1996).
19. M. É. Andrades, A. Morina, S. Spasić, I. Spasojević, Bench-to-bedside review: sepsis-from the redox point of view. *Crit. Care* **15**, 230 (2011).
20. P. E. Marik, V. Khangoora, R. Rivera, M. H. Hooper, J. Catravas, Hydrocortisone, vitamin C, and thiamine for the treatment of severe sepsis and septic shock: A retrospective before-after study. *Chest* **151**, 1229–1238 (2017).
21. N. Lane, A unifying view of ageing and disease: The double-agent theory. *J. Theor. Biol.* **225**, 531–540 (2003).
22. A. Gaudin, M. Yemisci, H. Eroglu, S. Lepetre-Mouelhi, O. F. Turkoglu, B. Dönmez-Demir, S. Caban, M. F. Sargon, S. Garcia-Argote, G. Pieters, Squalenoyl adenosine nanoparticles provide neuroprotection after stroke and spinal cord injury. *Nat. Nanotechnol.* **9**, 1054–1062 (2014).
23. D. Sobot, S. Mura, S. O. Yesylevskyy, L. Dalbin, F. Cayre, G. Bort, J. Mougin, D. Desmaële, S. Lepetre-Mouelhi, G. Pieters, Conjugation of squalene to gemcitabine as unique approach exploiting endogenous lipoproteins for drug delivery. *Nat. Commun.* **8**, 15678 (2017).
24. L. Kotelevets, E. Chastre, J. Caron, J. Mougin, G. Bastian, A. Pineau, F. Walker, T. Lehy, D. Desmaële, P. Couvreur, A squalene-based nanomedicine for oral treatment of colon cancer. *Cancer Res.* **77**, 2964–2975 (2017).
25. F. Dormont, M. Rouquette, C. Mahatsekake, F. Gobeaux, A. Peramo, R. Brusini, S. Calet, F. Testard, S. Lepetre-Mouelhi, D. Desmaële, M. Varna, Translation of nanomedicines from lab to industrial scale synthesis: The case of squalene-adenosine nanoparticles. *J. Control. Release* **307**, 302–314 (2019).
26. D. Desmaële, R. Gref, P. Couvreur, Squalenoylation: A generic platform for nanoparticular drug delivery. *J. Control. Release* **161**, 609–618 (2012).
27. H. Esterbauer, M. Dieber-Rotheneder, G. Striegl, G. Waeg, Role of vitamin E in preventing the oxidation of low-density lipoprotein. *Am. J. Clin. Nutr.* **53**, 314S–321S (1991).
28. L. Hakanpaa, E. A. Kiss, G. Jacquemet, I. Miinalainen, M. Lerche, C. Guzmán, E. Mervaala, L. Eklund, J. Ivaska, P. Saharinen, Targeting β1-integrin inhibits vascular leakage in endotoxemia. *Proc. Natl. Acad. Sci.* **115**, E6467–E6476 (2018).
29. E. A. Azzopardi, E. L. Ferguson, D. W. Thomas, The enhanced permeability retention effect: A new paradigm for drug targeting in infection. *J. Antimicrob. Chemother.* **68**, 257–274 (2012).

30. B. Halliwell, J. M. Gutteridge, *Free Radicals in Biology and Medicine* (Oxford Univ. Press, USA, 2015).
31. A. Gaudin, O. Tagit, D. Sobot, S. Lepetre-Mouelhi, J. Mougin, T. F. Martens, K. Braeckmans, V. R. Nicolas, D. Desmaële, S. C. de Smedt, Transport mechanisms of squalenoyl-adenosine nanoparticles across the blood–brain barrier. *Chem. Mater.* **27**, 3636–3647 (2015).
32. H. F. Galley, Bench-to-bedside review: Targeting antioxidants to mitochondria in sepsis. *Crit. Care* **14**, 230 (2010).
33. M. Rouquette, S. Lepetre-Mouelhi, O. Dufrançais, X. Yang, J. Mougin, G. Pieters, S. Garcia-Argote, A. P. IJzerman, P. Couvreur, Squalene-adenosine nanoparticles: Ligands of adenosine receptors or adenosine prodrug? *J. Pharmacol. Exp. Ther.* **369**, 144–151 (2019).
34. D. J. Wadleigh, S. T. Reddy, E. Kopp, S. Ghosh, H. R. Herschman, Transcriptional activation of the cyclooxygenase-2 gene in endotoxin-treated RAW 264.7 macrophages. *J. Biol. Chem.* **275**, 6259–6266 (2000).
35. A. T. Jacobs, L. J. Ignarro, Lipopolysaccharide-induced expression of interferon-β mediates the timing of inducible nitric-oxide synthase induction in RAW 264.7 macrophages. *J. Biol. Chem.* **276**, 47950–47957 (2001).
36. R. Korhonen, A. Lahti, H. Kankaanranta, E. Moilanen, Nitric oxide production and signaling in inflammation. *Curr. Drug Targets Inflamm. Allergy* **4**, 471–479 (2005).
37. C. Brodie, P. M. Blumberg, K. A. Jacobson, Activation of the A2A adenosine receptor inhibits nitric oxide production in glial cells. *FEBS Lett.* **429**, 139–142 (1998).
38. D. Yang, Y. Zhang, H. G. Nguyen, M. Koupenova, A. K. Chauhan, M. Makitalo, M. R. Jones, C. S. Hilaire, D. C. Seldin, P. Toselli, The A2B adenosine receptor protects against inflammation and excessive vascular adhesion. *J. Clin. Invest.* **116**, 1913–1923 (2006).
39. S. L. Deshmane, S. Kremlev, S. Amini, B. E. Sawaya, Monocyte chemoattractant protein-1 (MCP-1): An overview. *J. Interferon Cytokine Res.* **29**, 313–326 (2009).
40. C.-W. Chow, M. T. Herrera Abreu, T. Suzuki, G. P. Downey, Oxidative stress and acute lung injury. *Am. J. Respir. Cell Mol. Biol.* **29**, 427–431 (2003).
41. G. Yuhai, Z. Zhen, Significance of the changes occurring in the levels of interleukins, SOD and MDA in rat pulmonary tissue following exposure to different altitudes and exposure times. *Exp. Ther. Med.* **10**, 915–920 (2015).
42. E. Sewerynek, D. Melchiorri, L. Chen, R. J. Reiter, Melatonin reduces both basal and bacterial lipopolysaccharide-induced lipid peroxidation in vitro. *Free Radic. Biol. Med.* **19**, 903–909 (1995).
43. E. Sewerynek, J. Wiktorska, M. Stuss, 6-methoxytryptophol reduces lipopolysaccharide-induced lipid peroxidation in vitro more effectively than melatonin. *J. Physiol. Pharmacol.* **62**, 677–683 (2011).
44. E. Snoeck, K. Ver Donck, P. Jacqmin, H. Van Belle, A. G. Dupont, A. Van Peer, M. Danhof, Physiological red blood cell kinetic model to explain the apparent discrepancy between adenosine breakdown inhibition and nucleoside transporter occupancy of draflazine. *J. Pharmacol. Exp. Ther.* **286**, 142–149 (1998).
45. U. Flögel, S. Burghoff, P. L. van Lent, S. Temme, L. Galbarz, Z. Ding, A. El-Tayeb, S. Huels, F. Bönner, N. Borg, C. E. Müller, W. B. van den Berg, J. Schrader, Selective activation of adenosine A2A receptors on immune cells by a CD73-dependent prodrug suppresses joint inflammation in experimental rheumatoid arthritis. *Sci. Transl. Med.* **4**, 146ra108 (2012).
46. B. E. Barton, J. V. Jackson, Protective role of interleukin 6 in the lipopolysaccharide-galactosamine septic shock model. *Infect. Immun.* **61**, 1496–1499 (1993).
47. L. Ulloa, M. Ochani, H. Yang, M. Tanovic, D. Halperin, R. Yang, C. J. Czura, M. P. Fink, K. J. Tracey, Ethyl pyruvate prevents lethality in mice with established lethal sepsis and systemic inflammation. *Proc. Natl. Acad. Sci. U.S.A.* **99**, 12351–12356 (2002).
48. D. A. Zisman, S. L. Kunkel, R. M. Strieter, W. C. Tsai, K. Bucknell, J. Wilkowski, T. J. Standiford, MCP-1 protects mice in lethal endotoxemia. *J. Clin. Invest.* **99**, 2832–2836 (1997).
49. M. L. Kruzel, Y. Harari, C.-Y. Chen, G. A. Castro, Lactoferrin protects gut mucosal integrity during endotoxemia induced by lipopolysaccharide in mice. *Inflammation* **24**, 33–44 (2000).
50. M. J. Parmely, W. Zhou, C. D. Edwards III, D. Borcherding, R. Silverstein, D. Morrison, Adenosine and a related carbocyclic nucleoside analogue selectively inhibit tumor necrosis factor-alpha production and protect mice against endotoxin challenge. *J. Immunol.* **151**, 389–396 (1993).
51. M. Majetschak, S. M. Cohn, J. A. Nelson, E. H. Burton, U. Obertacke, K. G. Proctor, Effects of exogenous ubiquitin in lethal endotoxemia. *Surgery* **135**, 536–543 (2004).
52. M. Soh, D.-W. Kang, H.-G. Jeong, D. Kim, D. Y. Kim, W. Yang, C. Song, S. Baik, I.-Y. Choi, S.-K. Ki, Ceria–Zirconia nanoparticles as an enhanced multi-antioxidant for sepsis treatment. *Angewandte Chemie* **129**, 11557–11561 (2017).
53. B. Shrum, R. V. Anantha, S. X. Xu, M. Donnelly, S. M. Haeryfar, J. K. McCormick, T. Mele, A robust scoring system to evaluate sepsis severity in an animal model. *BMC. Res. Notes* **7**, 233 (2014).
54. S. Schwager, M. Detmar, Inflammation and lymphatic function. *Front. Immunol.* **10**, 308 (2019).
55. F. Wu, K. Tyml, J. X. Wilson, iNOS expression requires NADPH oxidase-dependent redox signaling in microvascular endothelial cells. *J. Cell. Physiol.* **217**, 207–214 (2008).
56. A. Azzi, S. N. Meydani, M. Meydani, J. M. Zingg, The rise, the fall and the renaissance of vitamin E. *Arch. Biochem. Biophys.* **595**, 100–108 (2016).
57. T. Nakamura, M. Goto, A. Matsumoto, I. Tanaka, Inhibition of NF-κB transcriptional activity by α-tocopheryl succinate. *Biofactors* **7**, 21–30 (1998).
58. Y. J. Suzuki, L. Packer, Inhibition of NF-κ B DNA binding activity by alpha-tocopheryl succinate. *Biochem. Mol. Biol. Int.* **31**, 693–700 (1993).
59. M. Rosenblat, M. Aviram, Oxysterol-induced activation of macrophage NADPH-oxidase enhances cell-mediated oxidation of LDL in the atherosclerotic apolipoprotein E deficient mouse: Inhibitory role for vitamin E. *Atherosclerosis* **160**, 69–80 (2002).

Acknowledgments: We wish to thank P. Van Tassel for helpful corrections to the manuscript and F. Gobeaux of UMR 3685 for help with cryo-TEM imaging. **Funding:** The authors gratefully acknowledge the financial support from the 7th EuroNanoMed-II call for proposals, project NanoHeart no. ANR-16-ENM2-0005-01. This work was further supported by la Fondation pour la Recherche Médicale (FRM) grant no. ECO20160736101. **Author contributions:** F.D., M.V., P.C., designed the research. F.D., R.B., C.C., F.R., A.P., A.G., F.G., M.V. conducted experiments. F.D., F.R., F.G., M.V., P.C. analyzed the data. F.D. wrote the paper, and all authors reviewed the manuscript. **Competing interests:** The authors declare that they have no competing interests. **Data and materials availability:** All data needed to evaluate the conclusions in the paper are present in the paper and/or the Supplementary Materials. Additional data related to this paper may be requested from the authors.

Submitted 20 September 2019
Accepted 10 April 2020
Published First Release: 27 April 2020
Published 5 June 2020
10.1126/sciadv.aaz5466

Citation: F. Dormont, R. Brusini, C. Cailleau, F. Reynaud, A. Peramo, A. Gendron, J. Mougin, F. Gaudin, M. Varna, P. Couvreur, Squalene-based multidrug nanoparticles for improved mitigation of uncontrolled inflammation in rodents. *Sci. Adv.* **6**, eaaz5466 (2020).